Original

Hoppe, S.; Michl, A.; Weissmueller, J.; Mueller, S.:
Ab-initio modeling of electromechanical coupling at Si surfaces
In: Journal of Applied Physics (2014) AIP

DOI: 10.1063/1.4893375

Ab-initio modeling of electromechanical coupling at Si surfaces

Sandra Hoppe,[1] Anja Michl,[1,2] Jörg Weissmüller,[2,3] and Stefan Müller[1,a)]
[1]*Institute of Advanced Ceramics, Hamburg University of Technology, 21073 Hamburg, Germany*
[2]*Institute of Materials Research, Materials Mechanics, Helmholtz-Zentrum Geesthacht, 21502 Geesthacht, Germany*
[3]*Institute of Materials Physics and Technology, Hamburg University of Technology, 21073 Hamburg, Germany*

(Received 26 June 2014; accepted 6 August 2014; published online 20 August 2014)

The electromechanical coupling at the silicon (100) and (111) surfaces was studied via density functional theory by calculating the response of the ionization potential and the electron affinity to different types of strain. We find a branched strain response of those two quantities with different coupling coefficients for negative and positive strain values. This can be attributed to the reduced crystal symmetry due to anisotropic strain, which partially lifts the degeneracy of the valence and conduction bands. Only the Si(111) electron affinity exhibits a monotonously linear strain response, as the conduction band valleys remain degenerate under strain. The strain response of the surface dipole is linear and seems to be dominated by volume changes. Our results may help to understand the mechanisms behind electromechanical coupling at an atomic level in greater detail and for different electronic and atomic structures. © *2014 AIP Publishing LLC*.
[http://dx.doi.org/10.1063/1.4893375]

I. INTRODUCTION

Investigating the coupling between a material's electrical and mechanical properties may be helpful for numerous applications, for example, in the field of actuators. In semiconductor technology, strain engineering is useful for several purposes: The large piezoresistance effect obtained for bulk Si and Si nanowires (SiNWs) allows for the application of Si as strain, pressure, or acceleration sensors.[1–3] In addition, straining Si enhances carrier mobility in two ways.[4,5] First, the six-fold degeneracy of the bulk Si conduction band minimum (CBM) is partially lifted by the reduced crystal symmetry caused by anisotropic strain. This decreases intervalley scattering. Second, band warping caused by strain may increase the band curvature and thereby decrease the effective masses of the charge carriers. This enhancement in carrier mobility was confirmed by experiment[6] and by computation using non-local empirical pseudopotentials.[4] An improved electron or hole mobility may help to optimize the efficiency of metal-oxide-semiconductor field-effect transistors.[7]

Straining Si also allows for band gap tuning. The response of the bulk band structure to strain has been analyzed in Refs. 5, and 8–10, where a linear decrease (increase) of the conduction band valleys and the valence band maximum (VBM) with tensile (compressive) strain and a splitting between the light hole (LH) and the heavy hole (HH) valence bands were found. With reference to a potential application for sensitive optical and electromechanical sensors, the influence of strain on the SiNW band structure has been investigated theoretically and a direct-to-indirect band gap transition at −4% strain has been obtained.[11] The most common way of straining Si is the growth on a template SiGe film, which was initially deposited onto a Si wafer.[5]

A direct consequence of the strain dependence of the electronic structure of semiconductors is the response of the work function to strain. This response is of interest, for example, in relation to strain mapping on surfaces using Kelvin probe techniques (see, e.g., Refs. 12 and 13). Yet, this phenomenon has predominantly been investigated for metal surfaces. Various studies in this field examined the variation of the surface stress with superficial charge density with regard to the surface electronic structure,[14] relaxation,[15,16] and adatom adsorption.[17–19] This coupling between surface stress and charge density has been characterized by a coupling coefficient ς, which is related to the variation of the electrode potential, U, with tangential strain, e, via a Maxwell relation.[20,21] Given that the electrode potential of zero charge is closely connected to the work function of the neutral surface in vacuum,[22,23] ς can be calculated in terms of the work function strain response via *ab-initio* techniques without considering an electrolyte solution.[24]

For gold, good agreement between theoretical and experimental values for ς has been obtained.[24–26] Via cyclic deformation of a thin gold film on a polymer substrate and measurement of the potential variation, a value of −1.83 eV for the response parameter has been found,[26] which is very close to the one of −1.89 eV resulting from *ab-initio* calculations.[24] More recently, Albina *et al.*[27] calculated response parameters for various 4d metals and some 3d and 5d metals and obtained results in a range from −0.25 eV to −2.5 eV. They found a more pronounced work function strain response for more close-packed surfaces and a parabolic dependence of the response parameter on the d-band occupation. Further studies in this field also report a negative trend for the work function strain response of different metals, such as copper or tungsten (see, e.g., Refs. 28–30). In contrast to the negative

a)Author to whom correspondence should be addressed. Electronic mail: stefan.mueller@tuhh.de

response parameters found for transition metals, a positive work function strain response was obtained for Al surfaces via density functional theory (DFT) calculations.[31] This was attributed to the high electron density of Al.

To the best of our knowledge, studies on electromechanical coupling of semiconductors are scarce. Few results are available on the work function strain response of different Si structures: Leu *et al.*[3] studied the influence of strain on the work function and other electronic properties of Si nanowires. Regarding separately the change of the surface dipole and the intrinsic bulk electronic structure with strain, they obtained an overall increase (decrease) of the work function with tensile (compressive) strain. More recently, Qin *et al.*[32] applied first-principles calculations to study the electronic and mechanical behavior of silicene under uniform in-plane strain, yielding a monotonous increase in the work function for strains up to 15% and a slight decrease afterwards up to 18% strain. Surprisingly, up to now, no results have been reported on electromechanical coupling for clean surfaces of Si crystals.

As compared to metals, analyzing the work function strain response in Si requires a different approach. The much larger screening length of semiconductors implies that the impact of the surface on the electronic structure may be larger than in metals. The electrons may also be strongly localized in covalent or partly ionic bonds. Furthermore, the Fermi level does not represent an occupied state in the semiconductor band structure. It is therefore debatable whether the response parameter should be defined in terms of the work function or rather in dependence of the electron affinity or the ionization potential (IP). The purely covalent sp^3-hybridized bonds make Si an ideal candidate to analyze the influence of strain on the electronic structure of a material with localized electrons and discuss the differences to electromechanical coupling at metal surfaces. Silicon surfaces and their reconstructions have been thoroughly investigated concerning their atomic and electronic properties.[33–40]

In this paper, we investigate the electromechanical coupling at the Si(100) p(2 × 1) and the Si(111) 2 × 1 surfaces via DFT calculations. Different types of strain were applied to the surface slabs and the response of the ionization potential and the electron affinity to strain was evaluated. For this purpose, the VBM and CBM were obtained from bulk band structure calculations.

The paper is organized as follows: Theoretical background and important parameters for the DFT calculations are given in Sec. II. The chosen Si surface reconstructions are presented and the implementation of strain to the surface slabs is explained. Results for the response of the ionization potential and the electron affinity to strain are shown in Sec. III. Our findings are then discussed in Sec. IV and summarized in the conclusions in Sec. V.

II. METHODOLOGY

A. Computational details

The DFT calculations in this work were performed with the plane-wave program code VASP.[41–44] PAW pseudopotentials[45,46] were applied to describe the interaction between valence electrons and ionic cores. An energy cutoff of 350 eV was selected. To obtain accurate band structures for the determination of the VBM and the CBM, the Heyd-Scuseria-Ernzerhof (HSE) screened Coulomb hybrid functional[47–50] was employed for exchange and correlation energies. Table I compares the indirect Si bulk band gap $E_{\mathrm{gap}}^{\mathrm{ind}}$ obtained by us to theoretical and experimental results from literature.[51–53] Obviously, both the local density approximation (LDA)[54–56] and the GGA Perdew-Burke-Ernzerhof functional (PBE)[57] considerably underestimate the band gap, while HSE and the quasiparticle GW approximation[58] agree well with the experimental value.

The mixing coefficient and the screening parameter for the HSE functional were set to 0.25 and 0.2 $\mathrm{Å}^{-1}$, respectively. Gaussian smearing with a smearing width of 0.001 eV was used. During relaxation of the surface slabs and bulk cells, the ions were allowed to relax until the forces acting on them reached a value of less than 0.01 eV/Å, while the cell size was kept constant.

Bulk calculations were performed for the Si two-atom primitive cell with a Γ-centered Monkhorst-Pack[59] grid of 9 × 9 × 9 k-points. Via a Murnaghan fit with the converged calculation parameters, the equilibrium stress-free lattice constant $a_0 = 5.4345$ Å was obtained. This value is very close to the experimental result of 5.4307 Å.[60]

Both the Si(100) and the Si(111) surfaces were modeled in symmetric surface slabs with two atoms per layer. The slabs contained 12 and 18 atomic layers for the Si(100) and the Si(111) surfaces, respectively, and an at least 13 Å thick vacuum region to avoid interactions between adjacent surfaces. A grid of 5 × 9 × 1 k-points was employed for both surfaces. For these parameters, the ionization potential of the Si(100) p(2 × 1) surface was converged within 12 meV.

Throughout this work, all energetic quantities are defined with reference to the macroscopic average[61] of the electrostatic potential V_{ave} in the bulk region of the surface slabs. This quantity was obtained via post-processing of the LOCPOT file with the Quantum ESPRESSO package.[62] Following this definition, the vacuum level V_{vac} equals the surface dipole potential V_{dip}, which is the same convention as used in Ref. 31.

Figure 1 illustrates the determination of the two quantities whose response to strain was investigated in this work, namely the IP ξ and the electron affinity χ. They represent

TABLE I. Comparison of our results for the indirect Si bulk band gap $E_{\mathrm{gap}}^{\mathrm{ind}}$ to literature values.

		$E_{\mathrm{gap}}^{\mathrm{ind}}$ (eV)
This work	PBE	0.56
	HSE	1.15
Literature	LDA[a]	0.46
	PBE[b]	0.58
	HSE[b]	1.15
	GW[a]	1.23
	Experiment[c]	1.17

[a]Reference 51.
[b]Reference 53.
[c]Reference 52.

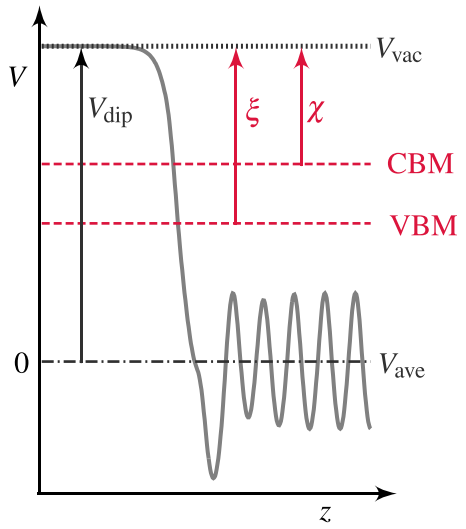

FIG. 1. Illustration of the determination of the surface dipole potential, V_{dip}, the ionization potential, ξ and the electron affinity, χ. The solid gray line represents the local electrostatic potential of a Si(100) p(2 × 1) surface slab along the surface normal z. The VBM and the CBM were obtained from band structure calculations along high symmetry points of the first Brillouin zone.

the difference between the surface dipole potential, V_{dip}, and the energy of the VBM, E_{VBM}, or the CBM, E_{CBM}, respectively

$$\xi = V_{dip} - E_{VBM} \quad (1)$$

$$\chi = V_{dip} - E_{CBM}. \quad (2)$$

For metal surfaces, the Fermi energy of the bulk cell equals that of the surface slab, if the latter incorporates sufficiently many layers. To overcome the often slow convergence of the surface slab Fermi energy with the number of atomic layers, the Fermi energy E_F is often obtained from bulk calculations and V_{dip} and E_F are referred to the average electrostatic potential, which serves as a common reference for bulk and surface calculations.[61,63] For the two reconstructed Si surfaces under consideration here, however, the highest occupied state would actually correspond to a dangling bond surface state within the bulk band gap. Thus, using the bulk VBM does not improve convergence here, but it leads to a different energy for the ionization potential compared to using the edge of the occupied surface state.

The dangling bond states, which arise from the surface reconstructions, are strongly localized at the Si surfaces. Only highly surface sensitive experimental methods manage to describe their position and dispersion adequately. Such methods include two-photon photoemission (2PPE),[40,64] inverse photoemission spectroscopy,[65,66] and angle-resolved photoemission spectroscopy (ARPES).[67–70] Furthermore, most experiments are carried out with doped Si samples instead of intrinsic ones. A possible space charge region at the surface may cause band bending, which makes the surface states difficult to investigate.[63]

To facilitate a straightforward comparability between our theoretical results and experimental values, we calculate the ionization potential and the electron affinity in terms of the bulk VBM and CBM, respectively. This also corresponds to the convention used in literature.

B. Silicon surface reconstructions

When Si is cleaved along the (100) plane, its surface reconstructs so that the topmost atoms form partly ionic asymmetric dimers with a charge transfer from the "down" to the "up" atom, which was first suggested by Chadi.[71] Thereby, the number of dangling bonds is reduced from two to one. This results in the formation of two electronic surface states within the bulk band gap.[67,70]

Among the possible reconstruction arrangements, the c(4 × 2) and the p(2 × 2) structures have been identified as the energetically lowest ones with a surface energy difference within the limit of accuracy of DFT.[37] The difference in surface energy to the p(2 × 1) asymmetric dimer reconstruction was calculated in this work to be less than 40 meV/1 × 1 cell. We chose the p(2 × 1) structure for our HSE calculations. In this way, we also optimized the amount of necessary computation time, as the p(2 × 1) unit cell contains only half the atoms of the p(2 × 2) or the c(4 × 2) unit cell. Atomic positions determined via DFT-LDA calculations[37] were used as a starting geometry for this surface. Four layers on each side of the surface slab were then allowed to relax in all three directions in order to find the equilibrium configuration without internal stresses. Figure 2(a) shows a side view of the p(2 × 1) reconstruction and illustrates the atom numbers and parameters used in Table II. As can be seen there, the resulting structure is in rather good agreement with low energy electron diffraction (LEED) results taken from

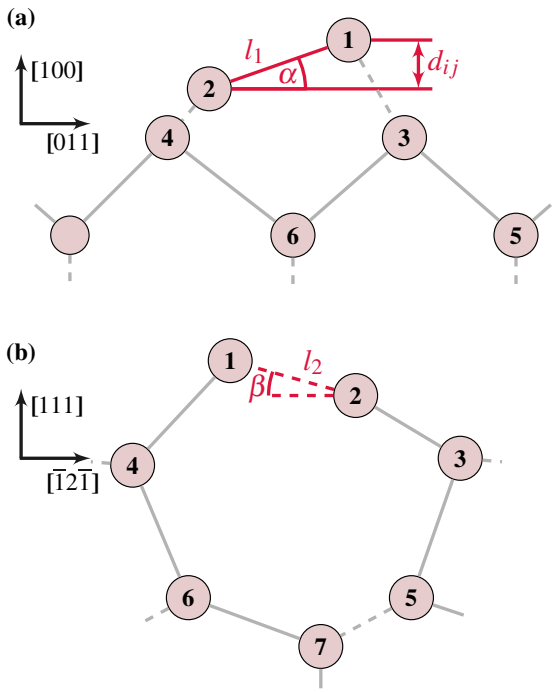

FIG. 2. Illustration of the reconstruction geometry for the Si(100) p(2 × 1) surface (a) and the Si(111) 2 × 1 surface (b). Atoms are numbered according to the notation in Table II. Further characteristic features of the surface reconstructions, i.e., buckling angles α and β as well as dimer bond length l_1 and π-chain atomic distance l_2 are depicted in light red. Solid lines are parallel to the plane of drawing.

TABLE II. Geometry of the Si surface reconstructions obtained in this work in comparison to experiment.[38,72] The values d_{ij} correspond to the vertical distances between the atoms in Figure 2. All lengths are given in Å.

	Si(100) p(2 × 1)		Si(111) 2 × 1	
d_{ij}	HSE	LEED[a]	HSE	LEED[b]
d_{12}	0.70	0.69	0.49	0.50
d_{23}	0.67	0.74	0.76	0.74
d_{34}	0.07	0.01	0.06	0.07
d_{45}	1.24	1.19	2.14	2.16
d_{56}	0.24	0.38	0.10	0.06
d_{67}	…	…	0.58	0.60
l_1	2.29	2.20	…	…
α [°]	17.70	18.28	…	…
l_2	…	…	2.28	2.27
β [°]	…	…	12.41	12.67

[a]Reference 38.
[b]Reference 72.

Table I in Ref. 38. Small deviations between our results and the considered LEED data may be attributed to the fact that the authors of Ref. 38 report a high defect concentration of their samples and achieve a moderate R_P factor (Pendry R factor) of 0.26.

The cleaved Si(111) surface exhibits a 2 × 1 reconstruction with π-bonded chains that was first proposed by Pandey in 1981.[73] His model was later corrected and a buckling of the outer chain and an overall compression were added.[33,74] Just like for the Si(100) p(2 × 1) surface, the reconstruction results in two surface states within the bulk band gap.[39,69] The ground state of the Si(111) surface is the well-known 7 × 7 reconstruction, which can be described by the dimer-adatom-stacking-fault (DAS) model.[36,75] Upon cleavage at temperatures below 417 °C, a metastable 2 × 1 reconstruction is formed.[76] The 2 × 1 reconstruction (Figure 2(b)) was chosen for this work for two reasons: First, computation time was reduced drastically and second, the mechanisms behind the response of electrical properties to applied strain can be identified more easily for a less complex surface structure.

The geometry of Ref. 33 obtained via LEED served as a starting point for our DFT calculations. Six atomic layers on each side of the surface slab were then allowed to relax in all three directions. We found a larger π-chain buckling of 0.49 Å in our calculations compared to the 0.38 Å in Ref. 33, but otherwise most atomic positions are in good agreement with the LEED results. This larger buckling was, however, also obtained via *ab-initio* calculations.[77–79] Table II shows excellent agreement between our results and a more recent LEED study,[72] which includes enhanced surface vibrations for the two π-chain atoms (atoms 1 and 2 in Figure 2(b)). Combining the experimental data from Ref. 33 with more recent methods of LEED analysis, the R_{RZJ} factor ("reduced" Zanazzi-Jona R factor) was reduced from 0.42 (Ref. 33) to 0.12 (Ref. 72).

C. Implementation of strain

Throughout this work, the equilibrium configurations of the bulk cells and the two surfaces in absence of strain and internal stresses (as described in Subsections II A and II B) with a lattice parameter of $a_0 = 5.4345$ Å were used as a reference for strain values. The response of the IP and electron affinity to mechanical strain was analyzed for different types of strain, which are illustrated in Figure 3.

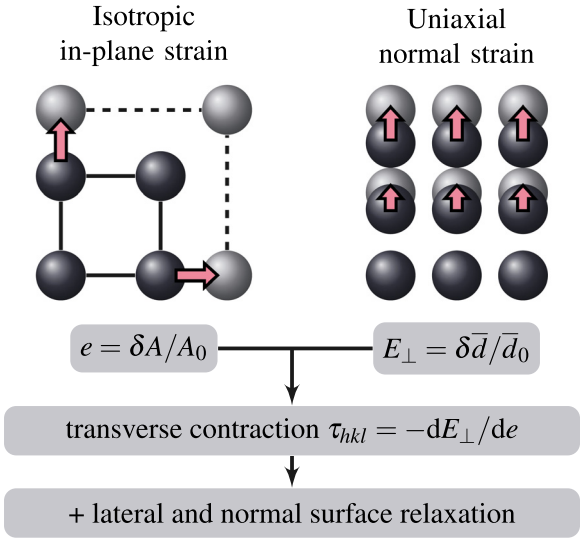

FIG. 3. Illustration of the applied strain types for a simple cubic structure. The transverse contraction tendency was considered by scaling the layer distances of the surface slabs under biaxial in-plane strain with $(1 - \tau_{hkl}e)$. Some layers on each side of the strained surface slabs were additionally allowed to relax in all three directions.

First, isotropic in-plane strain with values up to $|e| = 0.04$ was applied to the bulk cells and surface slabs, while the atomic layer distances in the direction of the surface normal z were kept fixed. The strain parameter $e = \delta A/A_0$ measures the relative area change, where A_0 is the area of the unstrained cell. Second, the bulk cells and surface slabs were subjected to pure uniaxial normal strain along z with values up to $|E_\perp| = 0.03$, where $E_\perp$ corresponds to a relative change in the layer distances $\delta\bar{d}/\bar{d}_0$. While it is reasonable to assume a homogeneous uniaxial strain distribution normal to the (100) plane, this is not the case for strain normal to the (111) plane. Layer distances along this direction can be divided into short and long ones, $\bar{d}_{\mathrm{short}}$ and $\bar{d}_{\mathrm{long}}$, respectively (Figure 4). The latter correspond to atomic bond lengths directly in the direction of the applied uniaxial strain. Compared to a homogeneous strain distribution, it is energetically more favorable to assign a larger portion of the overall normal strain to the atomic bonds within the short layer distances, which also contain components in the (111) plane. We therefore applied uniaxial strain along the [111] direction to bulk cells and let the atoms within the unit cell relax to find the equilibrium configuration. Our calculations show that the relative normal strain of the short layer distances is indeed about three times as large as that of the long ones.

In a next step, we considered a combination of in-plane strain and resulting transverse contraction. When in-plane strain is applied to a material, its dimension normal to the applied strain will not stay constant in the absence of forces in this direction. Bulk cells were subjected to in-plane strain in the (100) and in the (111) plane and the interlayer spacing $\bar{d}$ was varied systematically. For in-plane strain in the (111) plane, the atoms within the unit cell were again allowed to relax normal to the applied plane strain to obtain the equilibrium configuration. A quadratic fit was performed for the

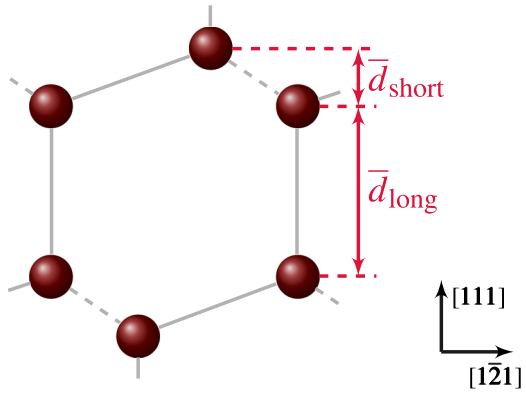

FIG. 4. Schematic illustration of the short and long layer distances $\bar{d}_{\text{short}}$ and $\bar{d}_{\text{long}}$, respectively, along the [111] direction. Solid lines are parallel to the plane of drawing.

calculated total energies vs. layer distance $\bar{d}$ in order to obtain the equilibrium bulk layer distance for a given e. The transverse contraction parameter τ_{hkl} thus describes the change in normal strain, in other words, in the mean bulk interlayer spacing in dependence of the applied in-plane strain for a given surface orientation

$$\tau_{hkl} = -\frac{\mathrm{d}E_\perp}{\mathrm{d}e}, \tag{3}$$

where hkl stands for the Miller indices. The value of τ_{hkl} for volume conservation in the limit of small strain would be 1. For Si(100), we found a transverse contraction parameter of 0.37, while it is only 0.21 for the Si(111) surface. These results agree with previous findings for the transverse elastic coupling at Si surfaces.[5] Interestingly, for an applied positive in-plane strain in the (111) plane, the long layer distances $\bar{d}_{\text{long}}$ along the [111] direction do not contract at all, but very slightly expand, while the short layer distances $\bar{d}_{\text{short}}$ strongly contract. This strain distribution was taken into account for the scaling of the layer distances, while along the [100] direction, the layer distances of the surface slabs under in-plane strain were accordingly scaled with $(1 - \tau_{hkl}e)$.

The strains discussed so far were imposed on the reference atomic configurations. Finally, additional surface relaxation of the strained surfaces along the surface normal z as well as in lateral directions was taken into account. Therefore, the outer four atomic layers of the Si(100) and six layers of the Si(111) strained surface slabs with scaled layer distances were allowed to relax in all three directions. This resulted in lateral displacements of up to 0.05 Å and displacements along the surface normal of up to 0.12 Å for the topmost atoms involved in the surface reconstructions.

The strain values assumed for Si in this work may seem inaccessible in experiments, but the response of the IP ξ and electron affinity χ to strain is expected to be linear for small strains. Hence, the magnitude of the slope of the linear fit equals that of the coupling coefficient ς. As described above, the relaxed slabs have undergone a homogeneous deformation in the surface plane as well as normal to the surface, followed by surface relaxation of the topmost atomic layers. Consequently, the dependency of the ionization potential on the applied strain can be decomposed as follows:

$$\xi = \xi^{\mathrm{h}}(e, E_\perp) + \Delta\xi^{\mathrm{rel}}(e, E_\perp), \tag{4}$$

where $\xi^{\mathrm{h}}(e, E_\perp)$ represents the ionization potential of the homogeneously strained slabs and $\Delta\xi^{\mathrm{rel}}(e, E_\perp)$ accounts for the difference between ξ and ξ^{h} due to surface relaxation. The analogous equation applies for the electron affinity. Regarding only homogeneous deformation, we denote the response of the IP and electron affinity to strain as $\mathrm{d}\xi/\mathrm{d}e|^{\mathrm{scaled}}$ and $\mathrm{d}\chi/\mathrm{d}e|^{\mathrm{scaled}}$, respectively. Coupling coefficients were calculated for all considered types of deformations, so that the response of the ionization potential to homogeneous strain can be decomposed as

$$\begin{aligned}\left.\frac{\mathrm{d}\xi}{\mathrm{d}e}\right|^{\mathrm{scaled}} &= \left.\frac{\partial\xi^{\mathrm{h}}}{\partial e}\right|_{E_\perp} + \left.\frac{\mathrm{d}E_\perp}{\mathrm{d}e}\,\frac{\partial\xi^{\mathrm{h}}}{\partial E_\perp}\right|_{e} \\ &= \left.\frac{\partial\xi^{\mathrm{h}}}{\partial e}\right|_{E_\perp} - \tau_{hkl}\left.\frac{\partial\xi^{\mathrm{h}}}{\partial E_\perp}\right|_{e},\end{aligned} \tag{5}$$

where $\partial\xi^{\mathrm{h}}/\partial e|_{E_\perp}$ and $\partial\xi^{\mathrm{h}}/\partial E_\perp|_e$ describe the response to pure in-plane strain with fixed layer distances and to normal strain with fixed in-plane dimensions, respectively. This decomposition of the strain response as well as the further consideration of strain relaxation allows us a more detailed view on the influence of strain on ξ and χ for silicon. Table III sums up all calculated response parameters for the types of strain described in this subsection.

III. RESULTS

Prior to elaborating on the strain response of the IP and the electron affinity, we present our results for IP and electron affinity of the unstrained Si surfaces and compare them to literature values (Table IV). Especially for the ionization potential, our DFT-HSE calculations are in good agreement with an experimental result for the Si(111) ionization potential from Ref. 80 and DFT-LDA/GW calculations performed by Sgiarovello *et al.*[79] Like the latter, we find smaller absolute values of the ionization potential and electron affinity for the Si(111) 2×1 surface than for the Si(100) $p(2 \times 1)$ surface. This trend contradicts Smoluchowski's rule,[81] which suggests a higher IP with increasing surface atomic packing for metals. Sgiarovello *et al.*[79] argue that atomic packing is not an adequate concept for Si surfaces, as the nearest neighbors of the surface atoms belong to the subsurface atomic plane. They instead attribute the larger IP of the Si(111) surface to a larger charge transfer from the vacuum to the surface bonding region than for the (100) surface.

TABLE III. Overview of the types of applied strain and the corresponding response parameters for the ionization potential ξ. The total strain response $\mathrm{d}\xi/\mathrm{d}e$ corresponds to the structure with scaled layer distances and surface relaxation.

Coefficient	Type of applied strain
$\partial\xi^{\mathrm{h}}/\partial e$	In-plane strain with fixed layer distances
$\partial\xi^{\mathrm{h}}/\partial E_\perp$	Uniaxial strain along the surface normal
$\mathrm{d}\xi/\mathrm{d}e\|^{\mathrm{scaled}}$	In-plane strain with scaled layer distances
$\mathbf{d\xi/de}$	In-plane strain with scaled layer distances and surface relaxation

TABLE IV. DFT-HSE results for ξ and χ of the unstrained Si(100) and (111) surfaces. All values are given in eV. The experimental result for the Si(100) ionization potential was measured for the c(4 × 2) reconstruction, which corresponds to a different arrangement of the tilted dimers.

	Si(100) p(2 × 1)		Si(111) 2 × 1	
	ξ	χ	ξ	χ
DFT-HSE	5.39	4.24	5.20	4.05
DFT-LDA/GW[a]	5.27	4.70	5.15	4.54
Experiment[b]	…	…	5.07	…
Experiment[c]	5.40	…	…	…

[a]Reference 79.
[b]Reference 80.
[c]Reference 40.

The results for the strain response of the ionization potential and electron affinity for the two surfaces, which are central findings of this paper, are summarized in Table V. Remarkably, our calculations reveal two branches and a change of sign of the electromechanical coupling coefficient for the transition from negative to positive applied strain. Figure 5 illustrates this finding, which is in striking contrast to various transition metals investigated in previous theoretical and experimental studies.[12,24,27,82] Only the strain response of the Si(111) electron affinity is monotonously linear with both positive and negative valued coupling coefficients. As visible in Figure 5, each branch is to good approximation a linear variation, which allows to determine the coupling coefficient via the slope of the linear fits.

Regarding first the Si(100) surface, the response parameters for ξ and χ are always of opposite sign in the respective strain regime. Consequently, with an increasing absolute value of tensile or compressive strain, the ionization potential decreases, whereas the electron affinity increases. Pure in-plane strain leads to the weakest response of ξ. While the absolute values of the coupling coefficients of the ionization potential are quite similar for $e < 0$ and $e > 0$, their difference is more pronounced for the electron affinity. This becomes most evident for uniaxial strain, where the transition from negative to positive strain results in a change of ς from −8.49 to 0.32 eV.

The branched response of the Si(111) ionization potential is less symmetrical than that of the (100) surface, i.e., coupling coefficients for negative strain have significantly larger magnitudes than those for positive strain. Unlike the (100) surface, the (111) surface exhibits a small positive response of 0.84 eV of the ionization potential for $e > 0$ and pure in-plane strain. The monotonously linear response of the electron affinity is most pronounced for uniaxial strain and only slightly negative for pure in-plane strain.

Allowing for relaxation of the surface layers has an impact on the response parameters of both surfaces. The relaxation process decreases the magnitude of the coupling coefficient of the ionization potential for $e < 0$ and increases it for $e > 0$, whereas the opposite holds for the Si(100) electron affinity.

A comparison between the interlayer distances for surface slabs with scaled layer spacings and with additional surface relaxation is given in Figure 6. Near the surface, the location of the layers was obtained by averaging over two atomic positions. The first atomic layer considered in this representation thus contains the dimer- and π-chain atoms, respectively. As there are short and long layer spacings in the [111] direction (Figure 4), they are examined in two separate diagrams. The impact of surface relaxation on both surfaces is most pronounced for the first layer distance, i.e., for the asymmetric dimer and π-chain atoms and the back bond atoms. For the (100) surface, the contraction of $\bar{d}_{12}$ for tensile strain is even stronger when surface relaxation is included. The long layer distances in the [111] direction stay nearly constant.

TABLE V. Calculated response parameters of the ionization potential and electron affinity for the types of strain described in Section II. All values are given in eV.

		Ionization potential	
		(100)	(111)
$\partial\xi/\partial e$	$(e<0)$	2.67	2.49
	$(e>0)$	−1.84	0.84
$\partial\xi/\partial E_\perp$	$(E_\perp<0)$	4.75	5.79
	$(E_\perp>0)$	−3.48	−4.63
$\mathrm{d}\xi/\mathrm{d}e\vert^{\mathrm{scaled}}$	$(e<0)$	3.81	5.49
	$(e>0)$	−3.33	−1.30
$\mathbf{d\xi/de}$	$(e<0)$	3.19	4.71
	$(e>0)$	−3.95	−2.08
		Electron affinity	
		(100)	(111)
$\partial\chi/\partial e$	$(e<0)$	−2.15	−0.18
	$(e>0)$	1.83	
$\partial\chi/\partial E_\perp$	$(E_\perp<0)$	−8.49	−3.10
	$(E_\perp>0)$	0.32	
$\mathrm{d}\chi/\mathrm{d}e\vert^{\mathrm{scaled}}$	$(e<0)$	−2.43	1.11
	$(e>0)$	5.00	
$\mathbf{d\chi/de}$	$(e<0)$	−3.05	0.33
	$(e>0)$	4.38	

IV. DISCUSSION

Previous studies on the influence of strain on the work function of SiNWs and silicene found a positive strain response.[3,32] While SiNWs exhibit a very strong work function strain response, it is less pronounced for silicene. In contrast to these one- and two-dimensional Si structures, the clean Si surfaces of our study exhibit a more complex behavior with a branched strain response and positive as well as negative coupling coefficients.

Intuitively, it seems reasonable that the energy necessary to extract an electron from the valence band, i.e., the ionization potential, decreases when the bonds are weakened and their bond lengths and bond angles are changed by applying tensile or compressive strain. Accordingly, one may expect an increase of the electron affinity, i.e., the energy gained for an electron entering the conduction band. Except for the Si(111) surface under pure in-plane strain and the monotonously linear response of the Si(111) electron affinity, our results confirm this expectation. To further analyze them, we can decompose the strain response of the ionization potential into the response of the dipole potential

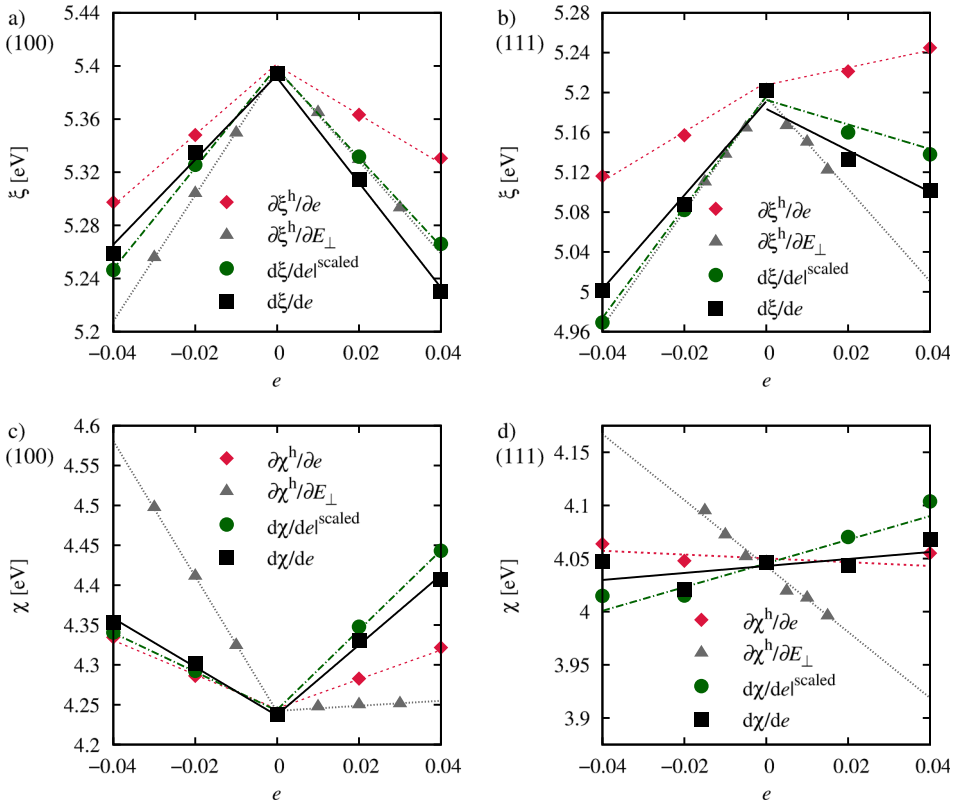

FIG. 5. Response of the Si(100) p(2 × 1) (a and c) and the Si(111) 2 × 1 (b and d) ionization potential and electron affinity to different types of applied strain. The strain response of the two quantities is to good approximation linear for positive and negative strain, respectively. The response parameters in Table V were therefore obtained from the slopes of the linear fits.

V_{dip} and that of the VBM and discuss the two variations separately:

$$\frac{\mathrm{d}\xi}{\mathrm{d}e} = \frac{\mathrm{d}V_{\mathrm{dip}}}{\mathrm{d}e} - \frac{\mathrm{d}E_{\mathrm{VBM}}}{\mathrm{d}e}. \tag{6}$$

The analogous decomposition is possible for the electron affinity, replacing E_{VBM} with E_{CBM} in Eq. (6). As we defined the ionization potential and electron affinity in terms of the bulk VBM and CBM, we can discuss the strain response of the latter without considering surface phenomena. Furthermore, the change of the coupling coefficients when surface relaxation is included is only caused by a variation of $\mathrm{d}V_{\mathrm{dip}}/\mathrm{d}e$.

The bar chart in Figure 7 presents the impact of the different applied strain types on V_{dip}, E_{VBM} and E_{CBM} for both surfaces for e, $E_\perp > 0$. The total response parameter for uniaxial strain $\mathrm{d}\xi/\mathrm{d}E_\perp$ is exemplarily included in the lower diagram. For both positive and negative applied strain, ς corresponds to the difference between two negative quantities. Despite some quantitative differences in the respective contributions to the strain response, both surfaces behave qualitatively similar regarding influence of the type of strain on the response of V_{dip}, E_{VBM}, and E_{CBM}. We will now elaborate further on the two contributions to ξ and χ, namely the dipole potential and the bulk band structure.

A. Response of V_{dip} to strain

The response of the surface dipole potential to strain is potentially influenced by two aspects: First, local dipoles on the surface caused by the surface reconstructions vary due to changes in the reconstruction geometry with applied strain. Second, the average charge density in the bulk material decreases with an increase in volume, which results in a decrease of the surface dipole, and vice versa. These two aspects will now be discussed in more detail. Our results for the strain response of V_{dip} are presented in Table VI.

When semiconductor surfaces reconstruct, electrons from dangling bonds are located in the surface bonding region and contribute to the formation of bulk-like bonds. The resulting charge redistribution lowers the surface's IP and reduces the magnitude of the surface dipole with respect to the bulk-truncated surface.[79] We calculated the surface dipoles for the bulk-truncated 1 × 1 surfaces and compared them to those of the reconstructed surfaces. The decrease in V_{dip} caused by the reconstruction was small for both surfaces, in other words the reconstruction process does not alter the surface dipole significantly. It is then not unreasonable to assume that small structural changes of the reconstructions due to applied strain also have a minor effect on V_{dip}.

To further examine this hypothesis, Table VII presents the relative variation of the dimer buckling and π-chain buckling d_{12} and the angles α and β (Figure 2) with respect to their equilibrium values. For both surfaces, the absolute values of these variations increase drastically when surface relaxation is included. Still, the strain response of V_{dip} changes only comparatively slightly (Table VI).

We now discuss the influence of the volume change on the strain response of V_{dip}. Despite the different bonding nature compared to metals, one can assign an average electron density to semiconductors, which is inversely proportional to their volume. According to their definition (Figure 3), isotropic in-plane strain e and normal strain $E_\perp$ both lead to the same amount of volume increase or decrease ΔV^{h}.

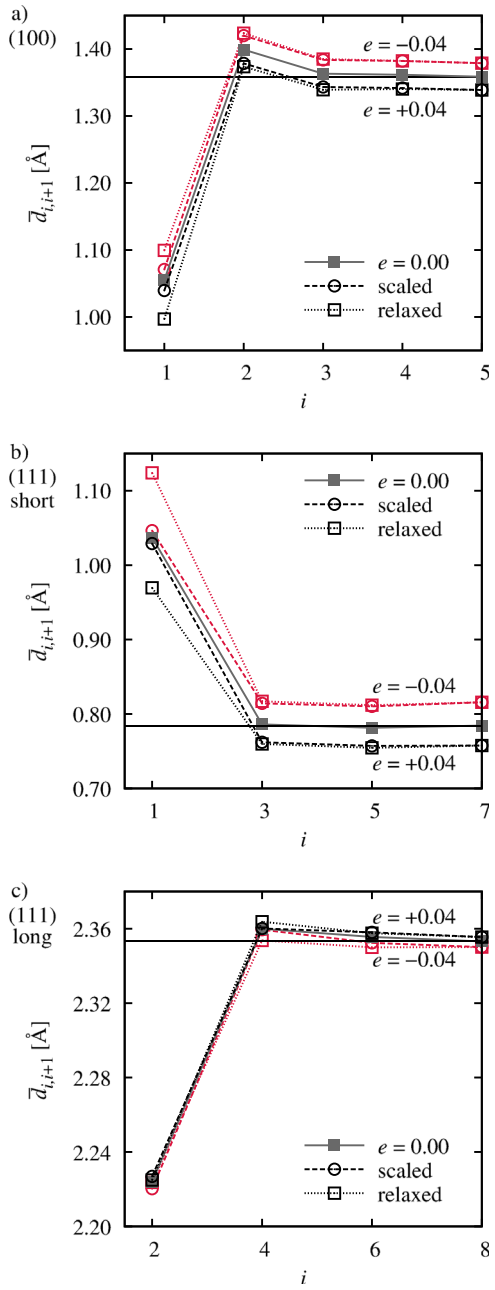

FIG. 6. Interlayer distances $\bar{d}_{i,i+1}$ for the first layers of the Si(100) (a) and Si(111) ((b) and (c)) unstrained surfaces and for surface slabs with scaled layer distances (dashed) and additional surface relaxation (dotted) with $e = \pm 0.04$. The solid horizontal lines illustrate the bulk equilibrium layer distances. The Si(111) surface possesses short and long layer spacings, which are depicted here in two diagrams ((111) short and (111) long, respectively) to provide a more detailed representation. Except for $\bar{d}_{12}$, the deviation from the structure with scaled layer distances is very small for both surfaces.

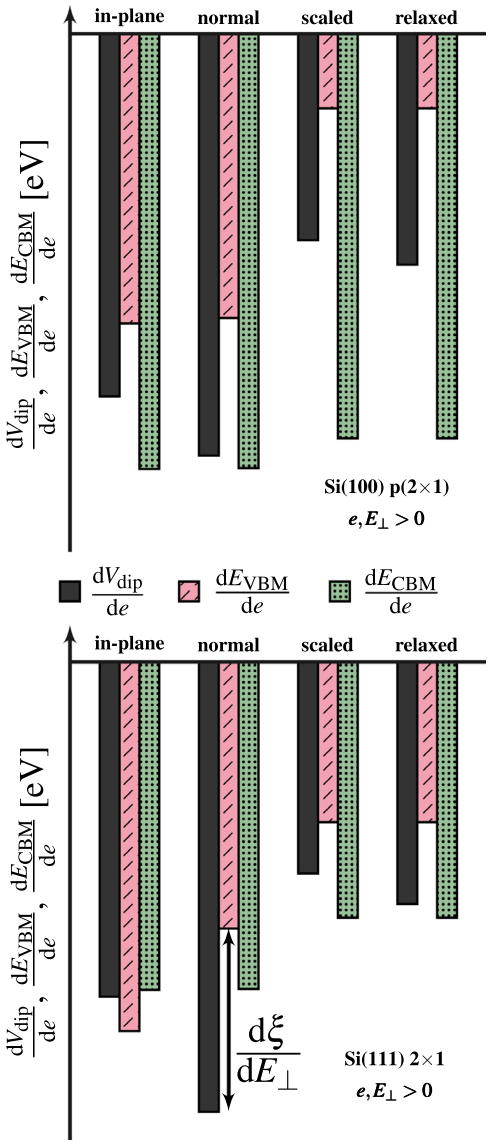

FIG. 7. To scale representation of the strain response of the surface dipole, VBM and CBM for the two surfaces for e, $E_\perp > 0$. The coupling coefficient $d\xi/dE_\perp$ is exemplarily included in the Si(111) diagram and represents the difference between two negative quantities. This also holds for e, $E_\perp < 0$ (not shown).

Moreover, we find that the volume of strained surface slabs with scaled layer distances stays nearly constant during additional surface relaxation. We therefore assign the same volume change ΔV^{sca} with respect to the unstrained surface to those slabs before and after the surface relaxation. Due to the scaling of the layer distances with τ_{hkl}, it applies $\Delta V^{h} > \Delta V^{sca}$. Especially regarding the Si(100) surface and to some extent also Si(111), the strain response of the surface dipole seems to be related to the volume change. A lower average electron density within the material caused by a positive volume change might result in a decreased surface dipole and vice versa.

However, our results suggest that the response of V_{dip} also depends on the degree of anisotropy of the applied strain. The charge transfer within the Si(100) p(2 × 1) asymmetric dimer is related to the amount of dimer buckling d_{12} and the buckling angle α (Figure 2).[83] Depending on the

TABLE VI. Strain response of the surface dipole potential for different types of strain. The largest negative response was obtained for normal strain for both surfaces. All values are given in eV.

	Si(100) p(2 × 1)	Si(111) 2 × 1
$\partial V^{h}_{dip}/\partial e$	−9.16	−8.45
$\partial V^{h}_{dip}/\partial E_\perp$	−10.65	−11.36
$dV_{dip}/de\|^{scaled}$	−5.21	−5.35
dV_{dip}/de	−5.83	−6.13

TABLE VII. Variation of characteristic surface reconstruction features d_{12}, α and β (Figure 2 and Table II) with strain and equilibrium values for the unstrained surfaces. Allowing for additional strain relaxation has a large influence on the change of the reconstruction geometry for both the Si(100) and the (111) surfaces.

Si(100) p(2 × 1)		
	$\frac{dd_{12}/d_{12,0}}{d...}$ [%]	$\frac{d\alpha/\alpha_0}{d...}$ [%]
e (in-plane)	0.0	−47.0
$E_\perp$ (normal)	100.0	93.8
$e\|^{\text{scaled}}$	−37.3	−81.8
e (surf. relaxation)	−149.2	−134.4
Equilibrium value	69.7 pm	17.7°
Si(111) 2 × 1		
	$\frac{dd_{12}/d_{12,0}}{d...}$ [%]	$\frac{d\beta/\beta_0}{d...}$ [%]
e (in-plane)	0.0	−48.4
$E_\perp$ (normal)	100.0	97.9
$e\|^{\text{scaled}}$	−21.2	−69.0
e (surf. relaxation)	−68.9	−345.6
Equilibrium value	49.0 pm	12.4°

nature of this relation, a larger normal strain may result in an increased charge transfer from the down- to the up-atom and thus in an increased surface dipole. Still, normal strain causes the strongest decrease of V_{dip} with strain for both surfaces. To analyze the influence of the dimer buckling on the surface dipole strain response, we calculated unstrained surface slabs with varying dimer buckling by slightly moving only the up-atom in the direction of the surface normal. Our calculations yielded a very small positive response of the surface dipole of 0.25 eV.

Comparing the impact of volume change on the surface dipole strain response with that of surface reconstruction deformation, changing the average electron density of Si seems to have a stronger effect than varying the local dipoles on the surface.

B. Response of the bulk band structure to strain

When bulk Si is subjected to non-hydrostatic strain, its cubic symmetry is lifted. Depending on the direction of the applied strain, this may result in the splitting of bands which are degenerate in the absence of strain. In silicon, the top three valence bands at the Γ point can be divided in bands of spin-orbit split-off (SO) hole, HH and LH. Biaxial strain in the {100} and {111} planes as well as uniaxial strain along the ⟨100⟩ and ⟨111⟩ directions partially lift the degeneracy of these three bands.[9]

In the absence of strain, the conduction band minimum consists of six Δ_6 valleys along the ⟨100⟩ directions. As these valleys are orientated symmetrically around the cubic unit cell diagonal, biaxial strain in the {111} planes and uniaxial strain along the ⟨111⟩ directions do not lift the band valley degeneracy. This fact explains the monotonously linear response of the Si(111) electron affinity to strain. All other types of strain mentioned above split the Δ_6 valleys into four in-plane Δ_4 valleys and two out-of-plane Δ_2 valleys.[9,84,85]

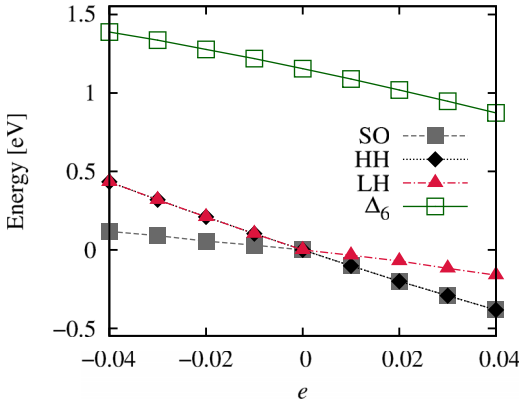

FIG. 8. Variation of the Si valence and conduction band edges as a function of biaxial strain in the (111) plane with scaled layer distances. The energy is given with reference to the VBM in the absence of strain.

Yu *et al.*[9] studied the influence of biaxial strain in the (100) plane on the valence and conduction bands of bulk Si. Analogous to their definition, we will from now on refer to the top valence bands as SO, HH, and LH in the order of ascending energy. Our findings regarding the strain response of the VBM and the CBM to biaxial strain in the (100) plane with scaled layer distances are in very good agreement with their results, taking into account that they presumably used the one-directional change of the lattice constant in their representation as strain parameter, which corresponds to 0.5e for small strains.

Similar to the diagram in Ref. 9 for biaxial strain in the (100) plane, Figure 8 shows our results for the strain response of the valence and conduction band edges for biaxial strain in the (111) plane with scaled layer distances. As relativistic corrections for the valence electrons were not taken into account in our calculations, the SO band is degenerate with the HH and the LH bands in the absence of strain. However, this should not affect the slope of the band edge variation with strain.

For biaxial strain in the (111) plane with scaled layer distances, we find a change in the slope of the strain response of the VBM at the transition from negative to positive strain (Figure 8). This result can be attributed to a crossover between bands.[9] The same argument applies for the CBM under biaxial strain in the (100) plane and uniaxial strain along the [100] direction. Therefore, this behavior of the VBM and the CBM was obtained for all types of strain, except for the strain response of the CBM to strain in the (111) plane or along the [111] direction. The different magnitudes of the strain responses of the VBM and the CBM (Figure 7) probably arise from the strongly directional covalent bonds in Si. The influence of an applied type of strain on the electronic structure is thus more pronounced for certain lattice distortions than for others.

V. CONCLUSIONS

In this work, we aimed to clarify the mechanisms behind electromechanical coupling at an atomic level and for

different electronic and atomic structures. For the Si surfaces under consideration, the Fermi level does not represent an occupied state and lies between the occupied and the unoccupied surface state in the surface band structure. Instead of calculating the work function strain response, like it has been done for metals as well as silicene and silicon nanowires, we have examined the strain response of the ionization potential and the electron affinity of two silicon surfaces.

Therefore, we performed surface calculations yielding the dipole potential and we obtained the VBM and CBM from bulk band structure calculations. We find a branched strain response of the ionization potential and electron affinity for positive and negative strain values and relatively large coupling coefficients compared to those of transition metals and aluminum.

The existence of these two branches can be explained in terms of the reduced cubic symmetry of the Si lattice. Only for biaxial strain in the (111) plane and uniaxial strain along the [111] direction, the degeneracy of the conduction band Δ_6 valleys is not lifted and therefore, the strain response of the electron affinity is monotonously linear in that case. We attribute the different magnitudes of the strain response of the VBM and the CBM for the different types of applied strain to the strongly directional covalent bonds in Si.

Apart from a small influence of the local dipoles at the surface that arise due to the reconstructions, the strain response of the surface dipole potential seems to be dominated by volume contributions.

Even though we discuss several hypotheses to explain the obtained results, the electromechanical coupling behavior at Si surfaces remains complex and several questions are still to be solved. In order to gain a deeper understanding, this topic might be investigated for different reconstructions or different semiconductors.

ACKNOWLEDGMENTS

We gratefully acknowledge the critical reading of the manuscript and the valuable scientific advice by Professor Dr. Thomas Fauster, Chair of Solid State Physics, Friedrich-Alexander-University Erlangen-Nürnberg in Germany.

[1]M. Tortonese, R. C. Barrett, and C. F. Quate, Appl. Phys. Lett. **62**, 834 (1993).
[2]R. He and P. Yang, Nat. Nanotechnol. **1**, 42 (2006).
[3]P. W. Leu, A. Svizhenko, and K. Cho, Phys. Rev. B **77**, 235305 (2008).
[4]M. V. Fischetti and S. E. Laux, J. Appl. Phys. **80**, 2234 (1996).
[5]M. Bouhassoune and A. Schindlmayr, Phys. Status Solidi C **7**, 460 (2010).
[6]K. Ismail, M. Arafa, K. L. Saenger, J. O. Chu, and B. S. Meyerson, Appl. Phys. Lett. **66**, 1077 (1995).
[7]B. M. Haugerud, L. A. Bosworth, and R. E. Belford, J. Appl. Phys. **94**, 4102 (2003).
[8]D. Rideau, M. Feraille, L. Ciampolini, M. Minondo, C. Tavernier, H. Jaouen, and A. Ghetti, Phys. Rev. B **74**, 195208 (2006).
[9]D. Yu, Y. Zhang, and F. Liu, Phys. Rev. B **78**, 245204 (2008).
[10]T. Maegawa, T. Yamauchi, T. Hara, H. Tsuchiya, and M. Ogawa, IEEE Trans. Electron. Devices **56**, 553 (2009).
[11]D. Shiri, Y. Kong, A. Buin, and M. P. Anantram, Appl. Phys. Lett. **93**, 073114 (2008).
[12]W. Li, Y. Wang, and D. Y. Li, Phys. Status Solidi A **201**, 2005 (2004).
[13]W. Li and D. Y. Li, J. Appl. Phys. **99**, 073502 (2006).
[14]H. Ibach, Surf. Sci. Rep. **29**, 195 (1997).
[15]F. Weigend, F. Evers, and J. Weissmüller, Small **2**, 1497 (2006).
[16]Y. Umeno, C. Elsässer, B. Meyer, P. Gumbsch, and J. Weissmüller, Europhys. Lett. **84**, 13002 (2008).
[17]W. Haiss, R. J. Nichols, J. K. Sass, and K. P. Charle, J. Electroanal. Chem. **452**, 199 (1998).
[18]W. Haiss, Rep. Prog. Phys. **64**, 591 (2001).
[19]R. N. Viswanath and J. Weissmüller, Acta Mater. **61**, 6301 (2013).
[20]A. Y. Gokhshtein, Dokl. Akad. Nauk SSSR **187**, 601 (1969).
[21]J. Weissmüller and D. Kramer, Langmuir **21**, 4592 (2005).
[22]S. Trasatti, J. Electroanal. Chem. Interfacial Electrochem. **33**, 351 (1971).
[23]D. L. Rath and D. M. Kolb, Surf. Sci. **109**, 641 (1981).
[24]Y. Umeno, C. Elsässer, B. Meyer, P. Gumbsch, M. Nothacker, J. Weissmüller, and F. Evers, Europhys. Lett. **78**, 13001 (2007).
[25]M. Smetanin, R. N. Viswanath, D. Kramer, D. Beckmann, T. Koch, L. A. Kibler, D. M. Kolb, and J. Weissmüller, Langmuir **24**, 8561 (2008).
[26]M. Smetanin, D. Kramer, S. Mohanan, U. Herr, and J. Weissmüller, Phys. Chem. Chem. Phys. **11**, 9008 (2009).
[27]J.-M. Albina, C. Elsässer, J. Weissmüller, P. Gumbsch, and Y. Umeno, Phys. Rev. B **85**, 125118 (2012).
[28]H. R. Gong, Y. Nishi, and K. Cho, Appl. Phys. Lett. **91**, 242105 (2007).
[29]D. Sekiba, Y. Yoshimoto, K. Nakatsuji, Y. Takagi, T. Iimori, S. Doi, and F. Komori, Phys. Rev. B **75**, 115404 (2007).
[30]X. F. Wang, W. Li, J. G. Lin, and Y. Xiao, Europhys. Lett. **89**, 66004 (2010).
[31]A. Michl, J. Weissmüller, and S. Müller, J. Phys.: Condens. Matter **25**, 445012 (2013).
[32]R. Qin, C.-H. Wang, W. Zhu, and Y. Zhang, AIP Adv. **2**, 022159 (2012).
[33]F. J. Himpsel, P. M. Marcus, R. Tromp, I. P. Batra, M. R. Cook, F. Jona, and H. Liu, Phys. Rev. B **30**, 2257 (1984).
[34]R. J. Hamers, R. M. Tromp, and J. E. Demuth, Phys. Rev. B **34**, 5343 (1986).
[35]N. Roberts and R. J. Needs, Surf. Sci. **236**, 112 (1990).
[36]K. D. Brommer, M. Needels, B. Larson, and J. D. Joannopoulos, Phys. Rev. Lett. **68**, 1355 (1992).
[37]A. Ramstad, G. Brocks, and P. J. Kelly, Phys. Rev. B **51**, 14504 (1995).
[38]H. Over, J. Wasserfall, W. Ranke, C. Ambiatello, R. Sawitzki, D. Wolf, and W. Moritz, Phys. Rev. B **55**, 4731 (1997).
[39]M. Rohlfing and S. G. Louie, Phys. Rev. Lett. **83**, 856 (1999).
[40]C. Kentsch, M. Kutschera, M. Weinelt, T. Fauster, and M. Rohlfing, Phys. Rev. B **65**, 035323 (2001).
[41]G. Kresse and J. Hafner, Phys. Rev. B **47**, 558 (1993).
[42]G. Kresse and J. Hafner, Phys. Rev. B **49**, 14251 (1994).
[43]G. Kresse and J. Furthmüller, Comput. Mater. Sci. **6**, 15 (1996).
[44]G. Kresse and J. Furthmüller, Phys. Rev. B **54**, 11169 (1996).
[45]P. E. Blöchl, Phys. Rev. B **50**, 17953 (1994).
[46]G. Kresse and D. Joubert, Phys. Rev. B **59**, 1758 (1999).
[47]J. Heyd, G. E. Scuseria, and M. Ernzerhof, J. Chem. Phys. **118**, 8207 (2003).
[48]J. Heyd and G. E. Scuseria, J. Chem. Phys. **121**, 1187 (2004).
[49]J. Heyd, J. E. Peralta, G. E. Scuseria, and R. L. Martin, J. Chem. Phys. **123**, 174101 (2005).
[50]J. Heyd, G. E. Scuseria, and M. Ernzerhof, J. Chem. Phys. **124**, 219906 (2006).
[51]M. Rohlfing, P. Krüger, and J. Pollmann, Phys. Rev. B **52**, 1905 (1995).
[52]C. Kittel, *Introduction to Solid State Physics* (John Wiley & Sons, Inc., New York, 1996).
[53]K. Hummer, J. Harl, and G. Kresse, Phys. Rev. B **80**, 115205 (2009).
[54]L. Hedin and B. I. Lundqvist, J. Phys. C **4**, 2064 (1971).
[55]D. M. Ceperley and B. J. Alder, Phys. Rev. Lett. **45**, 566 (1980).
[56]J. P. Perdew and A. Zunger, Phys. Rev. B **23**, 5048 (1981).
[57]A. E. Mattsson, R. Armiento, P. A. Schultz, and T. R. Mattsson, Phys. Rev. B **73**, 195123 (2006).
[58]L. Hedin, Phys. Rev. **139**, A796 (1965).
[59]H. J. Monkhorst and J. D. Pack, Phys. Rev. B **13**, 5188 (1976).
[60]M. A. Hopcroft, W. D. Nix, and T. W. Kenny, J. Microelectromech. Syst. **19**, 229 (2010).
[61]C. J. Fall, N. Binggeli, and A. Baldereschi, J. Phys.: Condens. Matter **11**, 2689 (1999).
[62]P. Giannozzi, S. Baroni, N. Bonini, M. Calandra, R. Car, C. Cavazzoni, D. Ceresoli, G. L. Chiarotti, M. Cococcioni, I. Dabo, A. D. Corso, S. de Gironcoli, S. Fabris, G. Fratesi, R. Gebauer, U. Gerstmann, C. Gougoussis, A. Kokalj, M. Lazzeri, L. Martin-Samos, N. Marzari, F. Mauri, R. Mazzarello, S. Paolini, A. Pasquarello, L. Paulatto, C. Sbraccia, S. Scandolo, G. Sclauzero, A. P. Seitsonen, A. Smogunov, P. Umari, and R. M. Wentzcovitch, J. Phys.: Condens. Matter **21**, 395502 (2009).
[63]H. Jiang and Y.-C. Shen, J. Chem. Phys. **139**, 164114 (2013).
[64]M. Weinelt, M. Kutschera, R. Schmidt, C. Orth, T. Fauster, and M. Rohlfing, Appl. Phys. A **80**, 995 (2005).

[65]F. J. Himpsel and T. Fauster, J. Vac. Sci. Technol. A **2**, 815 (1984).
[66]P. Perfetti, J. M. Nicholls, and B. Reihl, Phys. Rev. B **36**, 6160 (1987).
[67]R. I. G. Uhrberg, G. V. Hansson, J. M. Nicholls, and S. A. Flodström, Phys. Rev. B **24**, 4684 (1981).
[68]F. J. Himpsel, P. Heimann, and D. E. Eastman, Phys. Rev. B **24**, 2003 (1981).
[69]R. I. G. Uhrberg, G. V. Hansson, J. M. Nicholls, and S. A. Flodström, Phys. Rev. Lett. **48**, 1032 (1982).
[70]L. S. O. Johansson, R. I. G. Uhrberg, P. Mårtensson, and G. V. Hansson, Phys. Rev. B **42**, 1305 (1990).
[71]D. J. Chadi, Phys. Rev. Lett. **43**, 43 (1979).
[72]G. Xu, B. Deng, Z. Yu, S. Y. Tong, M. A. Van Hove, F. Jona, and I. Zasada, Phys. Rev. B **70**, 045307 (2004).
[73]K. C. Pandey, Phys. Rev. Lett. **47**, 1913 (1981).
[74]H. Sakama, A. Kawazu, and K. Ueda, Phys. Rev. B **34**, 1367 (1986).
[75]K. Takayanagi, Y. Tanishiro, S. Takahashi, and M. Takahashi, Surf. Sci. **164**, 367 (1985).
[76]D. Zhao and D. Haneman, Surf. Sci. **418**, 132 (1998).
[77]F. Ancilotto, W. Andreoni, A. Selloni, R. Car, and M. Parrinello, Phys. Rev. Lett. **65**, 3148 (1990).
[78]J. E. Northrup, M. S. Hybertsen, and S. G. Louie, Phys. Rev. Lett. **66**, 500 (1991).
[79]C. Sgiarovello, N. Binggeli, and A. Baldereschi, Phys. Rev. B **64**, 195305 (2001).
[80]S. M. Chérif, J.-P. Lacharme, and C. A. Sébenne, Surf. Sci. **274**, 257 (1992).
[81]R. Smoluchowski, Phys. Rev. **60**, 661 (1941).
[82]J. Weissmüller, R. N. Viswanath, L. A. Kibler, and D. M. Kolb, Phys. Chem. Chem. Phys. **13**, 2114 (2011).
[83]K. Hata, Y. Shibata, and H. Shigekawa, Phys. Rev. B **64**, 235310 (2001).
[84]T. Vogelsang and K. R. Hofmann, Appl. Phys. Lett. **63**, 186 (1993).
[85]C. Euaruksakul, Z. W. Li, F. Zheng, F. J. Himpsel, C. S. Ritz, B. Tanto, D. E. Savage, X. S. Liu, and M. G. Lagally, Phys. Rev. Lett. **101**, 147403 (2008).